Electron nongyrotropy in the context of collisionless magnetic reconnection

Nicolas Aunai, Michael Hesse, and Maria Kuznetsova

Citation: Physics of Plasmas (1994-present) **20**, 092903 (2013); doi: 10.1063/1.4820953
View online: http://dx.doi.org/10.1063/1.4820953
View Table of Contents: http://scitation.aip.org/content/aip/journal/pop/20/9?ver=pdfcov
Published by the AIP Publishing

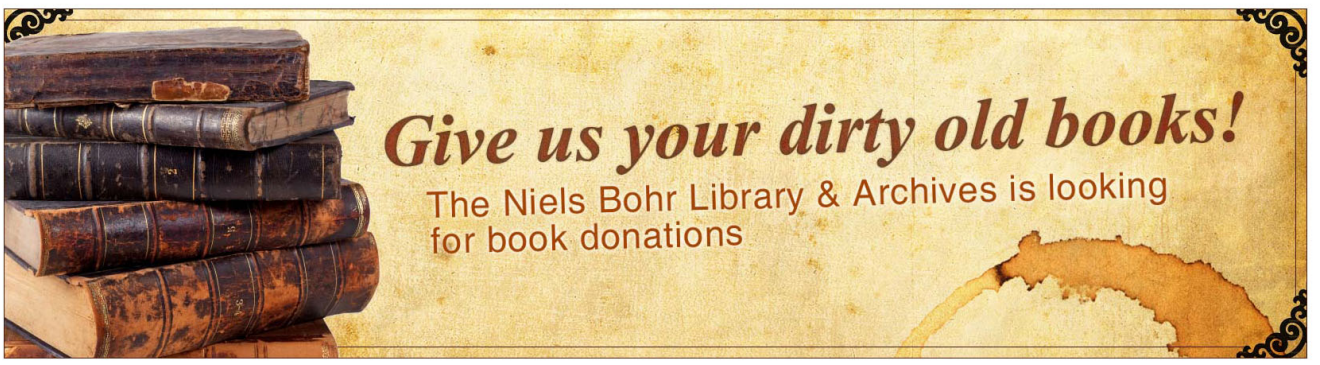

Electron nongyrotropy in the context of collisionless magnetic reconnection

Nicolas Aunai,[a] Michael Hesse, and Maria Kuznetsova
NASA Goddard Space Flight Center, Greenbelt, Maryland 20771, USA

(Received 23 July 2013; accepted 20 August 2013; published online 10 September 2013)

Collisionless magnetized plasmas have the tendency to isotropize their velocity distribution function around the local magnetic field direction, i.e., to be gyrotropic, unless some spatial and/or temporal fluctuations develop at the particle gyroscales. Electron gyroscale inhomogeneities are well known to develop during the magnetic reconnection process. Nongyrotropic electron velocity distribution functions have been observed to play a key role in the dissipative process breaking the field line connectivity. In this paper, we present a new method to quantify the deviation of a particle population from gyrotropy. The method accounts for the full 3D shape of the distribution and its analytical formulation allows fast numerical computation. Regions associated with a significant degree of nongyrotropy are shown, as well as the kinetic origin of the nongyrotropy and the fluid signature it is associated with. Using the result of 2.5D Particle-In-Cell simulations of magnetic reconnection in symmetric and asymmetric configurations, it is found that neither the reconnection site nor the topological boundaries are generally associated with a maximized degree of nongyrotropy. Nongyrotropic regions do not correspond to a specific fluid behavior as equivalent nongyrotropy is found to extend over the electron dissipation region as well as in non-dissipative diamagnetic drift layers. The localization of highly nongyrotropic regions in numerical models and their correlation with other observable quantities can, however, improve the characterization of spatial structures explored by spacecraft missions. © *2013 AIP Publishing LLC*. [http://dx.doi.org/10.1063/1.4820953]

I. INTRODUCTION

The velocity distribution function of a plasma population s, having a thermal energy E_{ths}, is said to be gyrotropic whenever it is invariant by rotation around the local magnetic field direction. Formally speaking, this condition can be translated in terms of an algebraic form of the population's pressure tensor $\mathbf{P}_s$

$$\mathbf{P}_s = \mathbf{G} \equiv P_\perp \mathbf{I} + (P_\parallel - P_\perp)\mathbf{bb}, \tag{1}$$

where $P_\parallel = \mathbf{bPb}$ is the thermal pressure along the magnetic field direction given by the unit vector $\mathbf{b}$, $P_\perp = E_{ths} - P_\parallel/2 = (Tr(\mathbf{P}_s) - P_\parallel)/2$. In case of gyrotropy, the full pressure tensor is therefore diagonal in any orthonormal basis $(\mathbf{b}, \mathbf{u}_{\perp 1}, \mathbf{u}_{\perp 2})$, which conveniently simplifies the fluid equations. Whenever Eq. (1) is not satisfied, the population is said to have a nongyrotropic distribution or simply to be nongyrotropic. Although the above definition of gyrotropy is exact, no real velocity distribution function satisfies it exactly. First, because the finite number of particles makes the perfect symmetry very unlikely; second, because even the slightest variations of physical quantities such as the density of the plasma, the magnetic field, etc., will locally result in small asymmetries in the velocity distribution function because of the local mixing of particles carrying slightly different phase space information. The concept of nongyrotropy is therefore not absolute but relative and what matters the most is how much a particle distribution is nongyrotropic, compared to another. In Vlasov systems, the number of particles per infinitesimal volume is so large that one may completely neglect its impact on the distribution's gyrotropy. We will see later on that this is not true anymore in Particle-in-Cell (PIC) simulations. Astrophysical Vlasov systems moreover usually develop inhomogeneities at much larger scales than the typical particle gyroscales. The magnetic field, binding particles to a particular flux tube, prevents the mixing of populations lying at distances further than their Larmor radius in the perpendicular direction, therefore ensures a certain degree of locality to the distribution functions, which naturally tend to be isotropic in the plane perpendicular to $\mathbf{b}$, i.e., tend to be gyrotropic.

Nongyrotropic plasmas have nevertheless been sometimes observed in collisionless systems.[1–3] They are associated with gradient length scales of the order of the particle gyro-radius and/or with unsteady wave-particle interactions on times scales comparable to the cyclotron time.[1] In both cases, detecting the nongyrotropic character of the plasma is important as it is a known source of instabilities and may help identifying spatial structures. In this paper, we investigate the nongyrotropic character of the electron population within the context of collisionless magnetic reconnection simulated with a 2.5D fully kinetic PIC code. Magnetic reconnection is perhaps the most well known and most important phenomena where nongyrotropic effects are playing a key role, since it is thought the macroscopic consequences of reconnection rely on the nongyrotropic electron behavior in a tiny region of space.[4] Recent studies[2,5–7] have emphasized the breaking of cylindrical symmetry of the distribution functions around the magnetic field direction that is

[a]nicolas.aunai@nasa.gov

associated with nongyrotropy in the context of magnetic reconnection. In this study, our goal is to establish a way to quantify the deviation of the full distribution function from gyrotropy, and then to understand which regions are, in this sense, more nongyrotropic than others, in the context of magnetic reconnection. We will then focus on understanding the kinetic origin of the observed nongyrotropy before looking at the associated fluid signatures.

II. NUMERICAL MODEL

The data presented in this paper have been obtained from fully kinetic, partially implicit, PIC simulations of collisionless magnetic reconnection. PIC codes solve the Vlasov-Maxwell system in a Lagrangian fashion, the code used in this study has already been described in a previously published article.[8] The data are normalized to characteristic ion scale constants. The density and the magnetic field are expressed in terms of an arbitrary density n_0 and magnetic field B_0. Distances are normalized by the ion inertial length $d_i = c/\omega_{pi}$, where $\omega_{pi}^2 = n_0 e^2/m_i \epsilon_0$ with ϵ_0 the vacuum permittivity, and c is the speed of light in vacuum. The time is normalized to the inverse of the ion cyclotron frequency Ω_{ci} based on the proton mass and charge and on B_0. The following results are obtained from two simulations, having a symmetric and an asymmetric initial condition in terms of the plasma and magnetic field values. The symmetric configuration is a simple Harris-like configuration, where the magnetic field is given by $\mathbf{B} = \tanh((z - z_0)/L)\mathbf{e}_x$, where $L = 0.5$ and z_0 is the simulation mid-plane. The density is $n(z) = 0.2 + \cosh^{-2}((z - z_0)/L)$. The plasma temperature is constant so is the electron to ion temperature ratio $T_e/T_i = 0.2$. The electron to ion mass ratio is $m_e/m_i = 100$ and the ratio between the electron plasma frequency and the electron cyclotron frequency is $\omega_{pe}/\Omega_{ce} = 4$. The domain size is $L_x = 64$ and $L_z = 30$ in the downstream and upstream directions, respectively. The number of cells is $(n_x, n_z) = (4096, 1600)$. The asymmetric simulation is the same as the one presented in a recent study.[9] It has an asymmetric profile of the density $n(z) = 1 - 1/3(\tanh((z - z_0)/L) + \tanh^2((z - z_0)/L))$ and of the magnetic field $\mathbf{B} = (0.5 + \tanh((z - z_0)/L))\mathbf{e}_x + 1\mathbf{e}_y$. The plasma temperature is identical to the symmetric run as is the electron to ion temperature ratio. The mass ratio is $m_e/m_i = 1/25$ and $\omega_{pe}/\Omega_{ce} = 4$. The domain size is (64, 25.6) with (1600, 800) cells. In both runs, the downstream boundaries are periodic and the upstream ones reflecting perfect conductors. A centered and localized perturbation is used to trigger magnetic reconnection.

III. MEASURING THE DEGREE OF NONGYROTROPY

Our first goal is to obtain a scalar measurement for the deviation of a distribution function from gyrotropy, so one can obtain a spatial visualization of which region is more nongyrotropic than another. Since nongyrotropy is a relative concept, we will call this scalar the *degree* of nongyrotropy of a given distribution function. In general, the full pressure tensor $\mathbf{P}_s$ of a particle species s does not satisfy Eq. (1). It can however always be decomposed as $\mathbf{P}_s = \mathbf{G} + \mathbf{N}$. This last equation defines $\mathbf{N}$ as the nongyrotropic part of the full pressure tensor $\mathbf{P}_s$. Since $Tr(\mathbf{P}_s) = Tr(\mathbf{G})$, it immediately follows that $Tr(\mathbf{N}) = 0$. If the velocity distribution function has a large degree of nongyrotropy, $\mathbf{G}$ does not represent it anymore but rather represents the pressure tensor of a virtual gyrotropic distribution function that would have the same thermal energy. The tensor $\mathbf{N}$ can therefore be seen as the deviation of the full distribution from that gyrotropic distribution. To be physically meaningfull, the degree of nongyrotropy should be independent of the basis in which the tensors are represented. A natural choice is to calculate the Frobenius norm $||\mathbf{N}||_F$, which in the case of a real symmetric tensor is given by $\sqrt{(\Sigma_i \lambda_i^2)}$, where λ_i are the eigenvalues of the tensor $\mathbf{N}$. Although the 3×3 eigenvalue problem is easily solved analytically and thus leads to a vectorized algorithm, one can show the Frobenius norm can also be written as $\sqrt{\sum_{i,j} N_{ij}^2}$, which leads to even faster computations. The local degree of nongyrotropy D_{ng} is obtained by normalizing this norm by the local thermal energy E_{ths}. We obtain the following equation:

$$D_{ng} = \frac{2\sqrt{\sum_{i,j} N_{ij}^2}}{Tr(\mathbf{P}_s)}. \tag{2}$$

It is important to note that D_{ng} given by Eq. (2) fully captures the degree of nongyrotropy of a velocity distribution in a sense that it measures the deviation of $\mathbf{P}_s$ from $\mathbf{G}$, representing the energetically equivalent gyrotropic distribution. Recent studies[2,5–7] have derived and used a scalar, called agyrotropy, representing the asymmetry of the distribution around the magnetic field by measuring the eccentricity of the ellipse associated with the covariance matrix of the velocity distribution projected onto the plane perpendicular to the magnetic field. If nongyrotropy is associated with an asymmetry of the distribution around the magnetic field, restricting the full 3D problem to the velocity dispersion in that plane may lead to a loss of information and result to incomplete predictions regarding which region is more nongyrotropic than another. For instance, one can imagine two distinct distribution functions which projections onto the perpendicular plane would be associated to ellipses with identical eccentricity although one 3D distribution may appear more gyrotropic than the other.

IV. ELECTRON NONGYROTROPY IN COLLISIONLESS MAGNETIC RECONNECTION

In a two-dimensional system, the reconnection electric field is supported by a nongyrotropic pressure gradient of both plasma species in the reconnection site area and has often been associated with a dissipative behavior.[4] Although in a three dimensional system, pressure variations may occur in the third direction; some simulations[10] have indicated that nongyrotropic distributions may play a role here also. Since electrons are lighter than protons, they are more difficult to unmagnetize and ultimately facilitate the reconnection of magnetic field lines, hence most reconnection studies focus

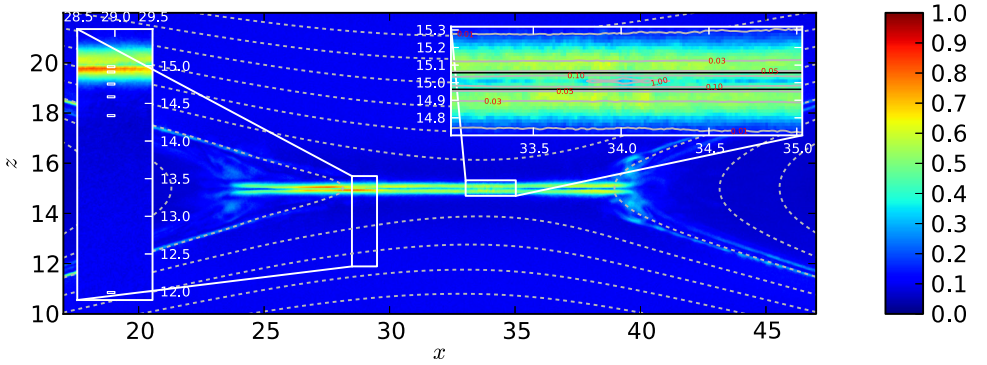

FIG. 1. Color representation of the nongyrotropy D_{ng} as calculated by Eq. (2). The dashed gray lines represent the in-plane magnetic field lines. The data have been averaged between $t = 30$ and $t = 30.075$, which represents 31 files. The upper right panel corresponds to a zoom in the reconnection site region. In this panel, the solid gray lines represent the isocontour of the thermal electron Larmor radius, which values are indicated on the contour lines. The two solid black lines represent the thermal electron bounce width, defined as the position where the thermal electron Larmor radius equals the local distance to the $B_x = 0$ line. The left panel is a zoom in the region inside the white rectangle at $x = 29$. It shows, as small white rectangles, the 6 boxes where particles are selected to make the distribution in Fig. 3.

on electron nongyrotropy rather than ion. In this section, we will use the previously described method to calculate and present where nongyrotropy occurs within the context of collisionless reconnection. We will then focus on the kinetic origin of the observed nongyrotropic regions, before investigating the fluid signatures they are associated with.

A. Where are electron distributions nongyrotropic?

Figure 1 shows, in color, the degree nongyrotropy D_{ng} for the electrons in a region surrounding the reconnection site of a symmetric configuration. The snapshot represents the state of the system, averaged between $t = 30$ and $t = 30.075$, which represents $30\,\omega_{pe}^{-1}$. At this time, the reconnection site is located inside the white rectangle at $x = 34$. The first thing we notice is that there is no region where the electrons are completely gyrotropic, i.e., where D_{ng} exactly zero, even in those where the ideal magnetohydrodynamics Ohm's law applies, like upstream of the X line. This finite and small value is not important and results from the overemphasized shot noise inherent to the PIC method. More important thus is the clear increase of the nongyrotropy as one gets closer to the mid-plane region. This region has already been highlighted by an agyrotropy scalar.[5,6] At the time of the snapshot, the narrow nongyrotropic band extends from $x \approx 24$ to $x \approx 40$. This extension is symmetric with respect to the initial location of the reconnection site $x = 32$ but not to its current location, which has slowly drifted to the right probably because of some asymmetry in the random particle initialization. This effect is also responsible for the small asymmetry between the structures of D_{ng} as $x \approx 24$ to $x \approx 40$. The influence of the periodic boundary is likely to be responsible for the stopping of the nongyrotropic layer in the downstream direction as will become clearer later on. The upper right panel of Fig. 1 represents a zoom in the area surrounding the X line and delimited by the white rectangle. This zoom reveals the nongyrotropic layer is slightly thicker than the electron bounce width represented on the figure by the two solid black lines and defined as the location where the distance from the neutral line ($B_x = 0$) equals the local thermal Larmor radius, based on a local proxy of the temperature $Tr(\mathbf{P}_e)/(3n_e)$, where n_e is the local electron density. The grey solid lines represent the contours of this local thermal Larmor radius and indicate it is much smaller where the nongyrotropy is maximum. This difference is probably due to the inconsistency between this isotropic electron temperature proxy and the real shape of the (nongyrotropic) distribution. Let us remark that, overall, nongyrotropic regions do not locate the X line region specifically nor they map topological boundaries.

The two panels of Fig. 2 present data from a simulation of asymmetric collisionless reconnection which results have

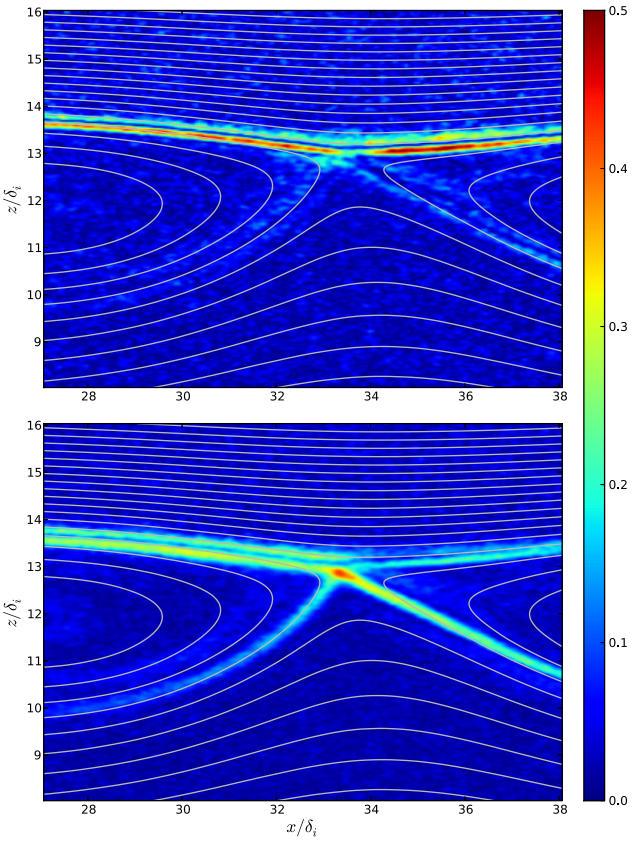

FIG. 2. The degree of nongyrotropy D_{ng} (bottom panel) is compared with the value of the agyrotropy scalar[5–7] (top panel), in the asymmetric configuration. The data are obtained at $t = 30.$ and spatially smoothed with a Gaussian filter to remove noise.

been already used in recently published articles.[9,11] Here, we compare the value of D_{ng} with the value of the agyrotropy scalar,[5–7] as the overall similarity of the structures visible on Fig. 1 with previous findings may suggest that both measures, although fundamentally different, are practically equivalent. The present panels clearly indicate this similarity may be a spurious consequence of the system symmetry, since in a more general, asymmetric and non coplanar configuration, they clearly differ. Although both measurements roughly agree on the gyrotropic regions, they differ in the relative amplitude of the nongyrotropy between the different regions where it is non-zero. Let us recall there is no clear, theoretical, definition of what should be a scalar coefficient of nongyrotropy as the exact definition of nongyrotropy involves the three-dimensional shape of the distribution function and is thus represented by tensorial relations. As our coefficient captures all this information, it is an appropriate scalar representation of the local nongyrotropy. In the present asymmetric simulation, we notice that D_{ng} is maximized in the area close to the reconnection site whereas the previously used measurement is not and is also more pronounced on the bottom separatrices. Contrary to the symmetric configuration, we see that this time, the separatrix regions have an enhanced nongyrotropy.

B. Origins of nongyrotropy from the kinetic viewpoint

We now investigate the kinetic origin of the observed nongyrotropy. Here, we focus on the symmetric configuration for simplicity, the non-ideal electron behavior in a region surrounding an asymmetric reconnection site, considerably more complicated, will be the topic of a forthcoming article. The left panel of Fig. 1 represents a zoom on a region located in the white rectangle at $x = 29$. In that zoom, we have represented six small rectangles of length 0.2 and width 0.05. These very small boxes constitute the selection areas of macroparticles to measure the velocity distribution function. The phase space density is averaged between $t = 30$ and $t = 30.075$ to increase the resolution. From bottom to top, distributions are labelled **a** to **f**. The distribution functions are shown in Fig. 3 in a projection onto the plane (V_y, V_z), which shows the most significant variation. For each distribution, we have represented the in-plane direction and amplitude of the bulk velocity, the direction of the local in-plane magnetic field, the value of the in-plane $\mathbf{E} \times \mathbf{B}/B^2$ drift velocity, and a gyrotropic ellipse, which axis is equal to three times the local parallel and perpendicular thermal velocities, based on the definition of $P_{\parallel}$ and $P_{\perp}$.

Distribution **a** lies in a region upstream of the separatrix and represents the incoming plasma. It is clearly an isotropic Maxwellian and is drifting very slowly toward the mid-plane ($V_z > 0$). Distributions **b** and **c** are downstream of the separatrix. They are clearly not isotropic however they are well fitted by the gyrotropic ellipse, consistently with the minimal value of D_{ng} in this region. The bulk velocity of the populations is close to the electromagnetic drift velocity $\mathbf{E} \times \mathbf{B}/B^2$. Note the magnetic field direction has not changed much and the main difference between the distributions concerns the parallel temperature, which is much larger than the

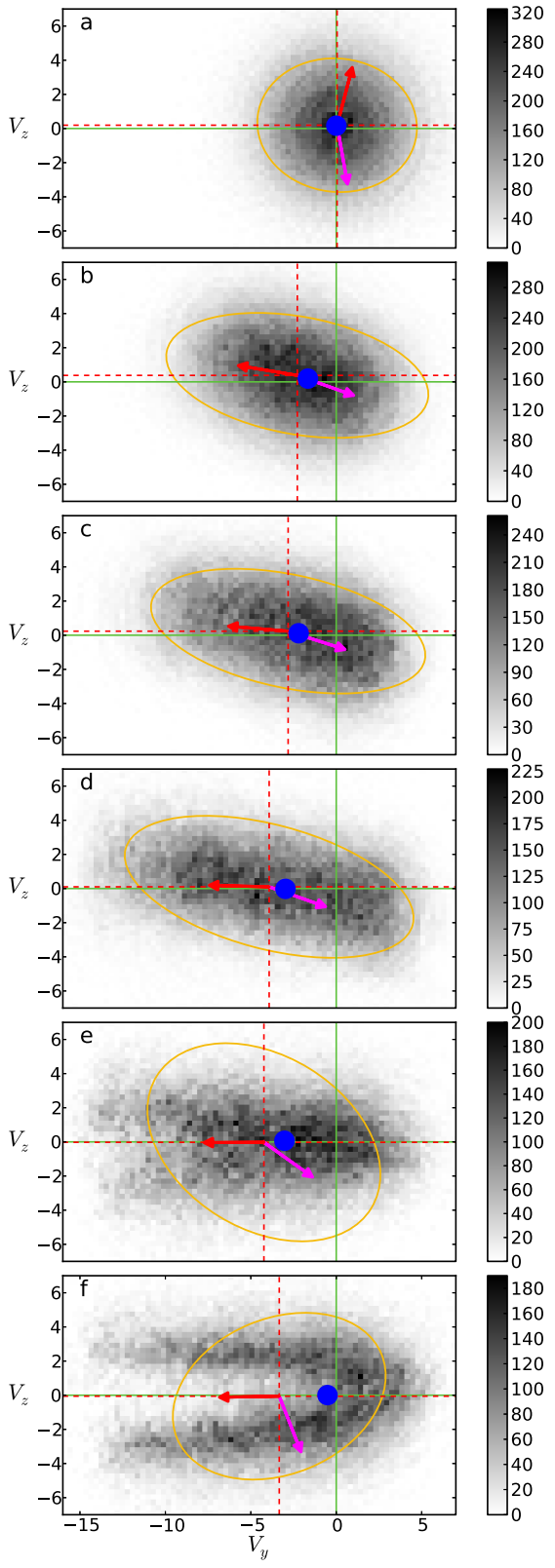

FIG. 3. Velocity distribution functions in the plane (v_y, v_z) averaged between $t = 30$ and $t = 30.075$. Distributions a to f are associated to the white rectangles on the left panel of Fig. 1, from bottom to top. The grey intensity represents the number of macroparticles in the velocity bin. The blue circle represents the in-plane $\mathbf{E} \times \mathbf{B}/B^2$. The red dashed horizontal and vertical lines indicate the position of the average in-plane velocity which direction is also indicated by the red arrow. The solid green line represents $V_y = V_z = 0$. The purple arrow represents the direction of the in-plane (B_y, B_z) magnetic field, and the axis of the yellow ellipse corresponds to the three times the thermal velocities parallel and perpendicular to the magnetic field.

perpendicular one and increases as one gets closer to the mid-plane region. Distribution **d** is located just below the border of the nongyrotropic region, its parallel temperature is even larger, and its shape is overall still reasonably well approximated by the associated gyrotropic ellipse which axis orientations, imposed by the local magnetic field, are still roughly unchanged. Distribution **e** is taken one step further in the nongyrotropic region. Consistently, one clearly sees the shape of the distribution is not regular anymore. The overall distribution is less tilted and one may notice the appearance of a gap at large V_y and small $|V_z|$. Note the principal axis of the distribution do not coincide anymore with those of the associated gyrotropic ellipse. The main reason lies in the rotation of the magnetic field, which, in this region, starts rotating due to the reversal of the B_y Hall quadrupolar component. As a result of this rotation, the perpendicular temperature of the virtual gyrotropic distribution artificially increases, constrained by the elongation of the real distribution in the V_y direction. The thermal energy being the same, the parallel temperature decreases. At this location, the bulk speed diverges from the electromagnetic drift, which decreases. Finally, distribution **f** is located at the simulation mid-plane. Due to spatial and temporal fluctuations, the rectangular selection area is not exactly symmetric around the $B_x = 0$ line, which explains why the magnetic field is still a bit oriented in the positive y direction. Its orientation has however much changed compared to location **e** and the gyrotropic ellipse associated with the local distribution has now a perpendicular temperature larger than the parallel one. The actual distribution here is fairly elongated in the y direction and the gap appearing already at location **e** has now become a clear evidence of counterstreaming electrons. At the exact symmetry line, the magnetic field would be completely in the z direction, the gyrotropic ellipse would have a very large perpendicular temperature compared to the parallel one and would match better the moments of the actual distribution, reducing its nongyrotropy, as seen on Fig. 1.

C. Nongyrotropic regions as seen from the fluid viewpoint

It is instructive to look at the fluid signatures in the regions of high nongyrotropy. Figure 4 consists of four panels, showing, from top to bottom, the degree of nongyrotropy D_{ng}, the electron bulk velocity in the x direction V_{ex}, the same component of the electron bulk velocity to which has been subtracted the x component of the electromagnetic $\mathbf{E}\times\mathbf{B}/B^2$ and diamagnetic drift velocities $\nabla\cdot\mathbf{P}_e\times\mathbf{B}/en_eB^2$, and finally a measure of non-ideal energy transfer[12] $D_e = \mathbf{j}\cdot(\mathbf{E}+\mathbf{v}\times\mathbf{B}) - \rho_c\mathbf{v}_e\cdot\mathbf{E}$. Consistently with several previous studies,[6,13–15] we observe an elongated electron jet layer. The jet disappears when the electromagnetic and diamagnetic drift velocities are subtracted. This v_{ex} bulk flow is associated with the current sustaining the reversal of the Hall quadrupolar and out-of-plane component of the magnetic field,[13] which consistently stops at the same locations $x \approx 24$ and $x \approx 40$. The non-ideal energy transfer occurs only in the

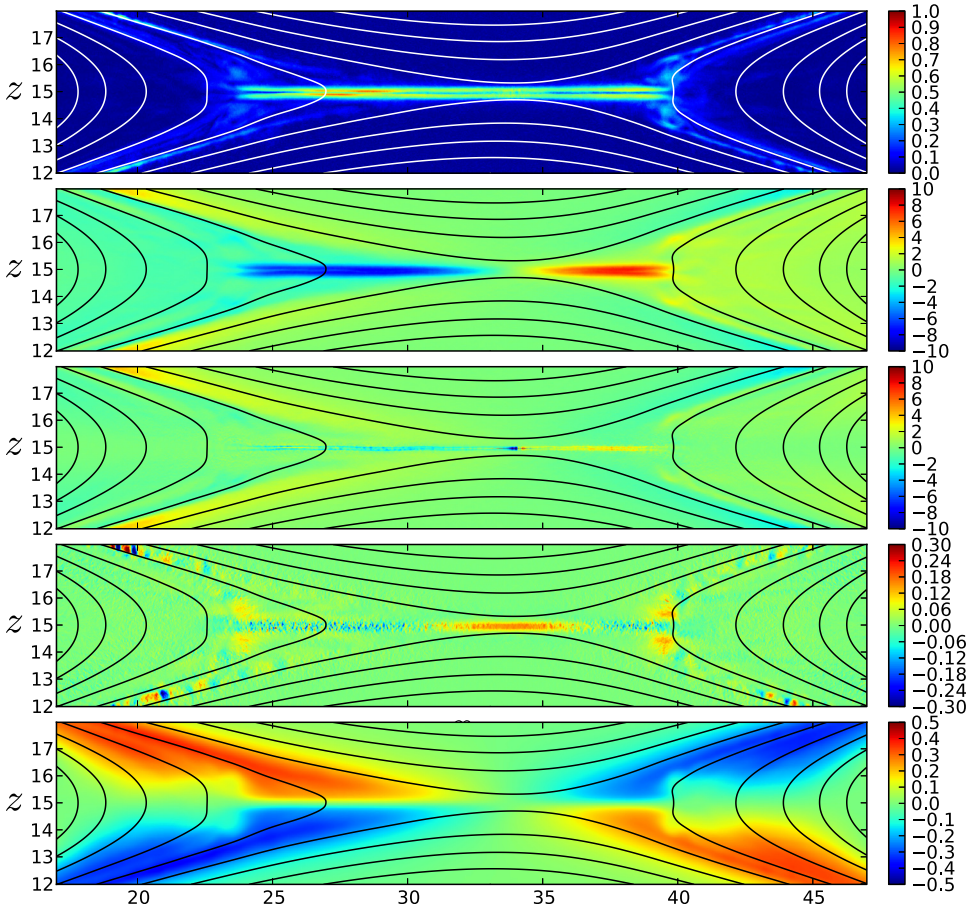

FIG. 4. From top to bottom: The degree of nongyrotropy already shown in 1 is reported here for comparison with other panels. The second panel shows the electron bulk velocity v_{ex}. The third panel shows v_{ex} from which has been subtracted the x component of the electromagnetic $\mathbf{E}\times\mathbf{B}/B^2$ and diamagnetic drift velocities $\nabla\cdot\mathbf{P}_e\times\mathbf{B}/en_eB^2$. The fourth panel shows a measure of non-ideal energy transfer[12] $D_e = \mathbf{j}\cdot(\mathbf{E}+\mathbf{v}\times\mathbf{B}) - \rho_c\mathbf{v}_e\cdot\mathbf{E}$. The bottom panel shows the out-of-plane magnetic field component. For each panel, the snapshot is made at $t = 30$, and the solid lines represent the in-plane magnetic field lines.

internal part of the layer, consistently with previous studies.[12,14] The clear evolution in the electron fluid behavior as one gets away from the X line is however not reflected in a variation of the degree of nongyrotropy, which stays roughly uniform. In other words, a significant degree of nongyrotropy does not seem to be a proxy of a specific fluid behavior. On the other hand, a specific fluid behavior like the diamagnetic drift, often presented in textbooks as the result of gyrating particles in an inhomogeneous plasma pressure, may be a degenerate macroscopic viewpoint of multiple kinetic mechanisms, including significantly nongyrotropic ones.

V. SUMMARY AND DISCUSSION

In this paper, we have presented a study of the plasma nongyrotropy within the context of collisionless magnetic reconnection, using fully kinetic PIC simulations. Because they ultimately facilitate the reconnection of magnetic field, we have focused on the electrons. In the first part of this work, we have presented a new method to quantify the degree of nongyrotropy of a local distribution function by measuring its deviation from the local, energetically equivalent, gyrotropic distribution. This method captures all the aspects of nongyrotropy associated with the 3D nature of the distribution and its analytical formulation allows its fast computation. Although it overall looks similar to the agyrotropy scalar in a symmetric configuration, a significant difference is seen in an asymmetric one. The analysis of both configurations lead us to the conclusion that nongyrotropy does in general not specifically map the reconnection site nor does it generally maps the topological boundaries, i.e., it can have substantial values within other regions. In a symmetric reconnecting system, the nongyrotropy originates from counterstreaming electrons populations in the region of rapidly rotating Hall magnetic field. The rotation of the magnetic field and the shape of the distribution function related to the electron bounce motion impose the variation of the degree of nongyrotropy. From the fluid viewpoint, the degree of nongyrotropy cannot be used alone as a proxy of a specific fluid behavior as regions of similar degree of nongyrotropy are associated to either the electron dissipation or diamagnetic drift layers. The rareness of regions with significant degree of nongyrotropy for the electrons however still make their localization in numerical models and correlation with other observable quantities interesting, as they can surely help in a better identification/characterization of spatial structures in spacecraft data. The NASA Magnetospheric MultiScale mission will have the resolution to measure electron scale variations of the pressure tensor, which makes the degree of nongyrotropy measurable.

ACKNOWLEDGMENTS

The authors kindly thank Deirdre Wendel for very useful discussions. N.A. acknowledges support from the NASA postdoctoral program. M.H. acknowledges support from the theory and modeling group of NASA's MMS.

[1]F. J. R. Simões, M. V. Alves, F. R. Cardoso, and E. Costa, J. Atmos. Sol.-Terr. Phys. **73**, 1511 (2011).
[2]J. D. Scudder, R. D. Holdaway, W. S. Daughton, H. Karimabadi, V. Roytershteyn, C. T. Russell, and J. Y. Lopez, Phys. Rev. Lett. **108**, 225005 (2012).
[3]L.-J. Chen, N. Bessho, B. Lefebvre, H. Vaith, A. Asnes, O. Santolik, A. Fazakerley, P. Puhl-Quinn, A. Bhattacharjee, Y. Khotyaintsev, P. Daly, and R. Torbert, Phys. Plasmas **16**, 056501 (2009).
[4]M. Hesse, T. Neukirch, K. Schindler, M. Kuznetsova, and S. Zenitani, Space Sci. Rev. **160**(1–4), 3 (2011).
[5]J. Scudder and W. Daughton, J. Geophys. Res. **113**, 06222, doi:10.1029/2008JA013035 (2008).
[6]H. Karimabadi, W. Daughton, and J. Scudder, Geophys. Res. Lett. **34**, 13104, doi:10.1029/2007GL030306 (2007).
[7]P. L. Pritchett and F. S. Mozer, J. Geophys. Res. **114**, 11210, doi:10.1029/2009JA014343 (2009).
[8]M. Hesse, J. Birn, and M. Kuznetsova, J. Geophys. Res. **106**, 3721, doi:10.1029/1999JA001002 (2001).
[9]N. Aunai, M. Hesse, S. Zenitani, M. Kuznetsova, C. Black, R. Evans, and R. Smets, Phys. Plasmas **20**, 022902 (2013).
[10]M. Hesse, M. Kuznetsova, K. Schindler, and J. Birn, Phys. Plasmas **12**, 100704 (2005).
[11]M. Hesse, N. Aunai, S. Zenitani, M. Kuznetsova, and J. Birn, Phys. Plasmas **20**, 61210 (2013).
[12]S. Zenitani, M. Hesse, A. Klimas, and M. Kuznetsova, Phys. Rev. Lett. **106**, 195003 (2011).
[13]M. Hesse, S. Zenitani, and A. Klimas, Phys. Plasmas **15**, 112102 (2008).
[14]S. Zenitani, M. Hesse, A. Klimas, C. Black, and M. Kuznetsova, Phys. Plasmas **18**, 122108 (2011).
[15]M. A. Shay, J. F. Drake, and M. Swisdak, Phys. Rev. Lett. **99**, 155002 (2007).